Papers

International Journal of Bifurcation and Chaos, Vol. 11, No. 1 (2001) 27–41

THE 1:2 MODE INTERACTION IN RAYLEIGH–BÉNARD CONVECTION WITH WEAKLY BROKEN MIDPLANE SYMMETRY

ISABEL MERCADER* and JOANA PRAT†
*Departament de Física Aplicada
†Departament de Matemàtica Aplicada i Telemàtica,
Universitat Politècnica de Catalunya, Barcelona, Spain

EDGAR KNOBLOCH
Department of Physics, University of California, Berkeley, CA 94720, USA

Received February 10, 2000; Revised March 22, 2000

The effects of weak breaking of the midplane reflection symmetry on the 1:2 steady state mode interaction in Rayleigh–Bénard convection are discussed in a PDE setting. Effects of this type arise from the inclusion of non-Boussinesq terms or due to small differences in the boundary conditions at the top and bottom of the convecting layer. The latter provides the simplest realization, and captures all qualitative effects of such symmetry breaking. The analysis is performed for two Prandtl numbers, $\sigma = 10$ and $\sigma = 0.1$, representing behavior typical of large and low Prandtl numbers, respectively.

1. Introduction

Midplane reflection symmetry plays a profound role in the theory of Rayleigh–Bénard convection. Its best known effect is the breaking of the degeneracy between up- and down-hexagons and the consequent preference for one or other hexagon type. This is because in three dimensions the loss of midplane reflection symmetry destabilizes convection in the form of parallel rolls and turns the bifurcation to hexagons into a transcritical bifurcation leading, at onset, to a hysteretic transition to one or other hexagon type. These effects are absent in systems with midplane reflection symmetry, i.e. systems in which the boundary conditions at the top and bottom are identical and non-Boussinesq effects are absent or ignored. It follows that the inclusion of non-Boussinesq terms or a change in the boundary conditions at the top results in a marked preference for hexagons [Busse, 1967] even though stable hexagons can and do occur in systems with exact reflection symmetry [Golubitsky *et al.*, 1984; Clever & Busse, 1996]. Since hexagons do not exist in two dimensions it is usually assumed that midplane symmetry plays no qualitative role in two dimensions. While this is indeed so for the transition to parallel rolls it is no longer true when mode interactions between n and $n+1$ rolls are considered. In this paper we discuss the most important of these mode interactions, the 1:2 interaction. This interaction has been studied abstractly, i.e. in the context of the amplitude equations governing the weakly nonlinear evolution of the modes, by Dangelmayr [1986] and, in more detail, by Armbruster *et al.* [1988], Jones and Proctor [1987], and Proctor and Jones [1988]. The analysis of these authors is based on the presence of the symmetry $O(2)$ arising from translations and reflection in a vertical plane when periodic boundary conditions are imposed in one direction. No midplane symmetry is therefore present. The authors identify different types of dynamical

behavior in the resulting normal form equations, including attracting structurally stable heteroclinic cycles. The corresponding problem with midplane reflection symmetry was considered by Busse and Or [1986] and Armbruster [1987] who showed that this type of behavior is absent in the corresponding normal form equations, and computed the required normal form coefficients for Boussinesq convection with stress-free boundaries at the top and bottom. Non-Boussinesq convection was studied by Manogg and Metzener [1994] from the same point of view, while Cox [1996] considered the long wave equations governing convection between nearly insulating boundaries with different combinations of stress-free and no-slip boundaries at the top and bottom.

Since the normal form analysis is necessarily limited in its applicability we consider in the present paper the full partial differential equations (PDEs) governing Boussinesq convection. This allows us to describe a larger neighborhood of the mode interaction point, while focusing at the same time on the effects of small symmetry breaking. We expect our results to capture *all* the effects of the breaking of the midplane reflection symmetry sufficiently close to the mode interaction point; moreover, we argue on the basis of genericity that the transitions that are found farther away from this point are also correctly described, although these need not all occur in any given problem. As a result our analysis also describes the effects of all small non-Boussinesq terms and small asymmetries in the boundary conditions such as those arising from the use at the top of Newton's law of cooling with a large Biot number. We anticipate that our results will also describe qualitatively convection in two-layer systems or other systems such as Bénard–Marangoni convection (e.g. [Echebarría *et al.*, 1997]) possessing a parameter that describes the extent to which the midplane symmetry is broken. Application to the interaction of turbulent boundary layers in narrow channels is also envisaged [Holmes *et al.*, 1996].

The paper is organized as follows. In Sec. 2 we summarize the equations and boundary conditions employed. The results obtained by numerical continuation are presented in Sec. 3 and focus on Prandtl numbers $\sigma = 10$ and 0.1, these being representative of high and low Prandtl number fluids. In Sec. 4 we provide a theoretical explanation of our results based on symmetry arguments. The paper concludes with a discussion in Sec. 5.

2. Basic Equations

We consider two-dimensional Boussinesq thermal convection in a periodic horizontal layer and include the possibility of generating a nontrivial mean flow. Consequently, we split the solenoidal velocity field $\mathbf{v}(x,\, z,\, t)$ into its mean and fluctuating components,

$$\mathbf{v} = \mathbf{U}(z,\, t) + \mathbf{v}'(x,\, z,\, t)\,,$$

where $\mathbf{U} = (U,\, 0)$, $\mathbf{v}' = (-\partial_z\chi',\, \partial_x\chi')$ and $\overline{\mathbf{v}}' = \overline{\chi}' = 0$, with the overline indicating an average over the horizontal period. The temperature $T(x,\, z,\, t)$ is written in the nondimensional form

$$T = \frac{1}{2} - z + \theta(x,\, z,\, t)\,.$$

Equations for U, χ' and θ are obtained from the horizontal average of the Navier–Stokes equations, the deviation of the vorticity equation from its horizontal average and the heat equation. In nondimensional form these are

$$(\partial_t - \sigma\partial_{zz}^2)U + \partial_z\overline{v_x' v_z'} = 0\,, \tag{1a}$$

$$(\partial_t + U\partial_x - \sigma\nabla^2)\omega' + Ra\,\sigma\partial_x\theta + \partial_{zz}^2 U\partial_x\chi' + \frac{\partial(\chi',\, \omega')}{\partial(x,\, z)} - \overline{\frac{\partial(\chi',\, \omega')}{\partial(x,\, z)}} = 0\,, \tag{1b}$$

$$(\partial_t + U\partial_x - \nabla^2)\theta - \partial_x\chi' + \frac{\partial(\chi',\, \theta)}{\partial(x,\, z)} = 0\,, \tag{1c}$$

where $\omega' = -\nabla^2\chi'$, lengths and time have been expressed in units of the layer depth and thermal diffusion time in the vertical, respectively, and Ra and σ are the Rayleigh and Prandtl numbers. The boundary conditions are taken to be periodic in x with period L. The top and bottom boundaries are perfectly conducting,

$$\theta = 0 \quad \text{at} \quad z = \pm\frac{1}{2}\,, \tag{1d}$$

with the velocity boundary conditions

$$\beta\partial_z U + (1-\beta)U = \chi' = \beta\partial_{zz}^2\chi' + (1-\beta)\partial_z\chi' = 0 \quad \text{at} \quad z = \frac{1}{2}\,, \tag{1e}$$

and

$$U = \chi' = \partial_z\chi' = 0 \quad \text{at} \quad z = -\frac{1}{2}\,. \tag{1f}$$

The equations are thus defined on the domain $(x, z) \in [0, L] \times [-1/2, 1/2]$. The resulting problem is solved numerically for $\beta = 0$ (the symmetric case) and $0 < \beta \ll 1$ (weakly broken midplane reflection symmetry) using a spectral Galerkin–Fourier technique in x and collocation-Chebyshev in z. In the following we define the quantity $\alpha \equiv 2\pi/L$ and compute bifurcation diagrams as a function of Ra for values of α on either side of α_c, the location of the 1:2 resonance. This point, $(Ra_c, \alpha_c) \approx (2022, 2.165)$, is determined by the intersection of the $n = 1$ and $n = 2$ neutral stability curves for the conduction state (see Fig. 1), and is independent of the Prandtl number and almost independent of β for the small values of β considered here.

Insight into the results can be gained by considering the symmetries of the basic states that emerge from the conduction state as Ra is increased, and the (usually smaller) symmetries of states created in subsequent (secondary) bifurcations. These symmetries depend on the presence or absence of the midplane reflection symmetry. When $\beta = 0$, Eqs. (1) are equivariant under the two reflections,

$$R_0 : (x, z) \to (-x, z), \ (U, \chi', \theta) \to (-U, -\chi', \theta), \tag{2a}$$

$$\kappa : (x, z) \to (x, -z), \ (U, \chi', \theta) \to (U, -\chi', -\theta), \tag{2b}$$

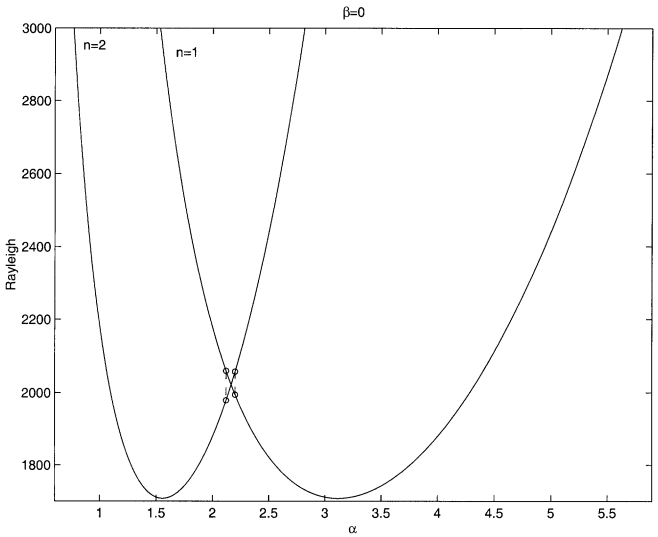

Fig. 1. The location of the 1:2 resonance in the (Ra, α) plane for Rayleigh–Bénard convection with no-slip boundary conditions. Here $\alpha = 2\pi/L$ and L is the spatial period: $Ra_c = 2021.6$, $\alpha_c = 2.1648$. The open circles indicate the location of the primary bifurcations when $\alpha = 2.12$ and $\alpha = 2.2$.

and translations through a distance ℓ,

$$T_\ell : (x, z) \to (x + \ell, z), \quad (U, \chi', \theta) \to (U, \chi', \theta). \tag{2c}$$

The reflection (2a) is with respect to an arbitrarily chosen origin in x; reflections R_{ℓ_0} with respect to a plane $x = \ell_0$, say, are obtained by conjugation: $R_{\ell_0} = T_{\ell_0} R_0 T_{-\ell_0}$. These symmetries generate the symmetry group $\Gamma = O(2) \times Z_2$. The conduction state $U = \chi' = \theta = 0$ is invariant under this group. The primary instability of this state is to a nontrivial roll state $(0, \chi', \theta)$ that breaks the translation symmetry T_ℓ but is invariant under a reflection R_{ℓ_0} for an appropriate ℓ_0 and the *shift-reflect* operation $T_{a/2}\kappa$, where $a \equiv L/n$ is the pattern wavelength [Prat *et al.*, 1998]. Each of these symmetries is a generalized reflection in the sense that its square is the identity. It follows that the symmetry group of such a roll state is $G \equiv Z_2 \times Z_2 = D_2$, a subgroup of $O(2) \times Z_2$ [Weiss, 1990; Moore *et al.*, 1991; Prat *et al.*, 1995]. In contrast an individual roll is invariant only under a 180° rotation. For a pattern with a node at $x = 0$ this symmetry is $P = R_{a/4}\kappa$ and is sometimes referred to as a *point* symmetry. This symmetry acts on the fields as follows:

$$\begin{aligned} P : (x, z) &\to \left(\frac{a}{2} - x, -z\right), \\ (U, \chi', \theta) &\to (-U, \chi', -\theta). \end{aligned} \tag{2d}$$

Note that $P = R_0 T_{a/2} \kappa$ (since $T_{\ell_0} R_0 T_{\ell_0} = R_0$) and so $P \in G$. In the following we shall use the symbol R to refer to the reflection R_{ℓ_0} for *suitable* ℓ_0.

When $\beta > 0$ the reflection κ is broken and $\Gamma = O(2)$. The symmetry of the primary flow is thus $G \equiv Z_2$, i.e. R [Crawford & Knobloch, 1991]. In either case the symmetry R of the primary flow implies that no mean flow is present: $U(z) \equiv 0$. This is not necessarily so for the states produced in secondary bifurcations from the primary rolls, if these break the symmetry R of the roll state.

When $\beta = 0$ the presence of the D_2 symmetry implies that a roll state of wavelength a can be written in the form

$$\chi'(x, z) = \sum_{k=1}^{K} \sum_{m=0}^{M} \chi_{km} f_m(2z) \sin\left(\frac{2\pi k x}{a}\right),$$

$$\theta(x, z) = \sum_{k=0}^{K} \sum_{m=0}^{M} T_{km} g_m(2z) \cos\left(\frac{2\pi k x}{a}\right),$$

relative to a suitable origin. Here $k+m$ is odd, and the functions $f_m(2z)$, $g_m(2z)$ are suitable combinations of Chebyshev polynomials satisfying the boundary conditions. These functions are odd when m is odd and even when m is even. The linear stability of such a roll state is determined as in [Prat *et al.*, 1995, 1998]. When $\beta = 0$ the possible perturbations split into four disjoint classes, those that are invariant under the full group $G \equiv D_2$, and those that are invariant under the three nontrivial subgroups of G generated by the generalized reflections P, $T_{a/2}\kappa$ and R, respectively [Prat *et al.*, 1998]. A zero eigenvalue with respect to perturbations of the first type indicates a saddle-node bifurcation. The next two classes of perturbations, P and $T_{a/2}\kappa$, generate solutions with antisymmetric and symmetric mean flow profiles $U(z)$, respectively. Steady state bifurcations of this type produce secondary branches of tilted cells, and of traveling waves. The remaining perturbation type results in a bifurcation to a secondary branch of solutions that are invariant under R; such solutions are not associated with a mean flow. Note that these conclusions apply to *fully* nonlinear roll states.

These considerations also apply to the state $n = 2$ provided perturbations of period $L/2$ are considered. However, in a domain of period L this state can also lose stability with respect to perturbations of wavelength L corresponding to an instability of $n = 2$ with respect to the state $n = 1$. Such an instability is a spatial subharmonic instability and is characterized by a Floquet multiplier $1/2$, cf. [Prat *et al.*, 1998]. It produces a secondary branch of solutions with smaller symmetry that can be computed using the expansion

$$U(z) = \sum_{m=0}^{M} U_m \tilde{g}_m(2z)\,,$$

$$\chi'(x,\, z) = \sum_{k=-K}^{K\,\prime} \sum_{m=0}^{M} \chi_{km} f_m(2z) e^{ik\alpha x}\,,$$

$$\theta(x,\, z) = \sum_{k=-K}^{K} \sum_{m=0}^{M} T_{km} g_m(2z) e^{ik\alpha x}\,,$$

with χ_{km} and T_{km} now complex and satisfying $\chi_{-km} = \chi^*_{km}$, $T_{-km} = T^*_{km}$. The prime indicates that the $k = 0$ term is absent. The stability of these solutions is calculated as for the D_2-symmetric rolls although the perturbations no longer split into four subgroups. Note that for $\beta = 0$, $\tilde{g}_m = g_m$; however, this is no longer so once $\beta > 0$ because $\tilde{g}_m$ now satisfies different boundary conditions than g_m.

We restrict the analysis that follows to solutions that are either steady, or that are steady in a suitably moving reference frame, i.e. to traveling waves (hereafter TW). The speed of the frame (the phase velocity c of the wave) is determined as part of the solution. All of these solutions (including the $n = 1$ steady state for $\beta \neq 0$) can be computed using the above general expansion, with x replaced by $x - ct$ for the TW. In all cases the symmetry properties guarantee the existence of TW solutions with phase velocity $\pm c$; the sign of c is therefore arbitrary. The computations employ a Newton–Raphson iterative scheme with $K \leq 16$, $M \leq 16$ or $M \leq 20$. This resolution suffices for the relatively modest values of the Rayleigh number considered because the Prandtl number used is not very small. For small values of β considered no Hopf bifurcations to standing waves were detected.

There is a fundamental reason for computing TW in problems of this type. This is because the breaking of the midplane reflection κ allows some of the secondary steady solutions to drift [Matthews *et al.*, 1992; Knobloch, 1996]. This is the case for the point-symmetric solutions P but not for the solutions with the symmetries R or G since both of these retain the symmetry R even with broken midplane reflection symmetry (see Sec. 4). However, TW can be produced in a secondary bifurcation even when $\beta = 0$, provided the instability breaks both the R and P symmetries that are then present. Of course, when $\beta > 0$ the shift-reflect symmetry of this state is lost but it remains a traveling wave. More details about the symmetries of the possible secondary solution branches can be found in [Prat *et al.*, 1998].

3. The Bifurcation Diagrams

Our results for $\sigma = 10$ are summarized in Figs. 2 and 3, and those for $\sigma = 0.1$ in Figs. 4 and 5. Of these the first figure in each case summarizes the results in schematic form, since the quantitative results presented in Figs. 3 and 5 mask some of the details. In these figures steady solutions are indicated by solid lines, while traveling waves are indicated by dashed lines. The figures also give the signs of the two dominant eigenvalues, with a minus sign indicating stability. The schematic figures consist of four bifurcation diagrams, showing the

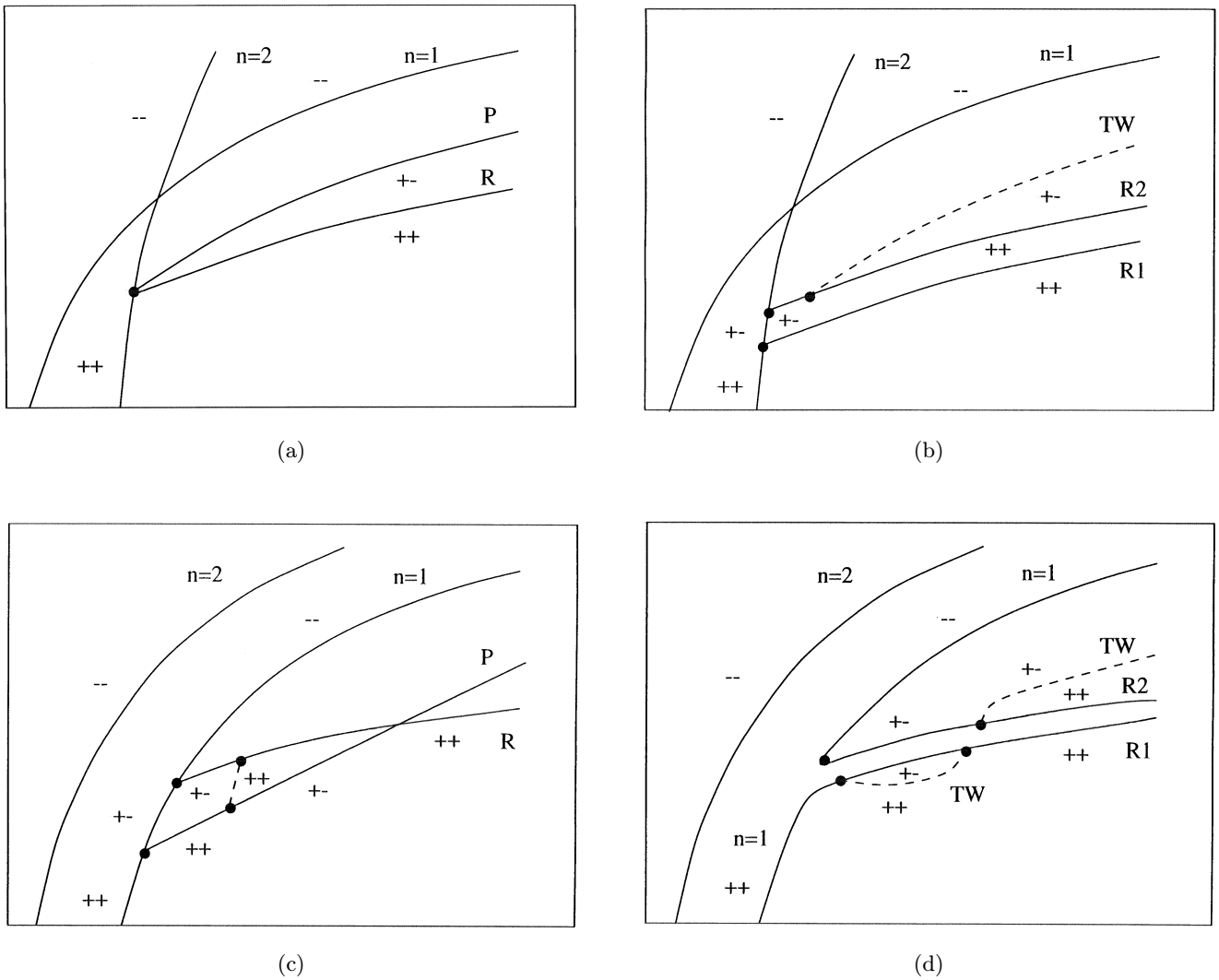

Fig. 2. Schematic bifurcation diagrams for $\sigma = 10$. (a) $\alpha = 2.2$, $\beta = 0$. (b) $\alpha = 2.2$, $\beta = 10^{-4}$. (c) $\alpha = 2.12$, $\beta = 0$. (d) $\alpha = 2.12$, $\beta = 10^{-5}$. The solid (dashed) lines denote steady (traveling) solutions. Secondary bifurcations are indicated by solid dots and stability by the signs of the two leading eigenvalues, with + (−) indicating instability (stability).

results for $\beta = 0$ and $0 < \beta \ll 1$ and the two choices $\alpha = 2.2 > \alpha_c$ and $\alpha = 2.12 < \alpha_c$. For $\alpha > \alpha_c$ the mode $n = 1$ sets in prior to $n = 2$ and vice versa; when $\beta = 0$ this is a pure mode, but this is no longer the case when $\beta > 0$, i.e. when $\beta > 0$ the $n = 1$ solutions contain some $n = 2$ contribution as soon as $Ra > Ra_c$. In contrast the $n = 2$ mode is always a pure mode (see Sec. 4). Since the distinction between $\beta = 0$ and $0 < \beta \ll 1$ is almost invisible in the Nusselt number plots shown in Figs. 3 and 5 these show the results for $\beta = 0$ only. Additional plots of the phase velocity of any traveling wave present are also included in these figures since these distinguish clearly between branches of steady and traveling solutions even if these have almost identical heat transport properties.

3.1. *Results for $\sigma = 10$*

Figure 2(a) summarizes the results for $\beta = 0$, i.e. for the problem with midplane symmetry, and $\alpha = 2.2 > \alpha_c$ shown in Fig. 3(a). The $n = 1$ mode bifurcates first and remains stable for all values of Ra. This bifurcation is closely followed by a bifurcation to the $n = 2$ mode; this state is initially unstable but gains stability already at small amplitude (as measured by $Nu - 1$, where Nu is the Nusselt number), when a pair of (unstable) secondary branches bifurcates from it. One of these, labeled P, is point-symmetric, while the other, labeled R, is symmetric with respect to the reflection R. Figure 6 indicates the form of the different types of solutions. No tertiary bifurcations to traveling

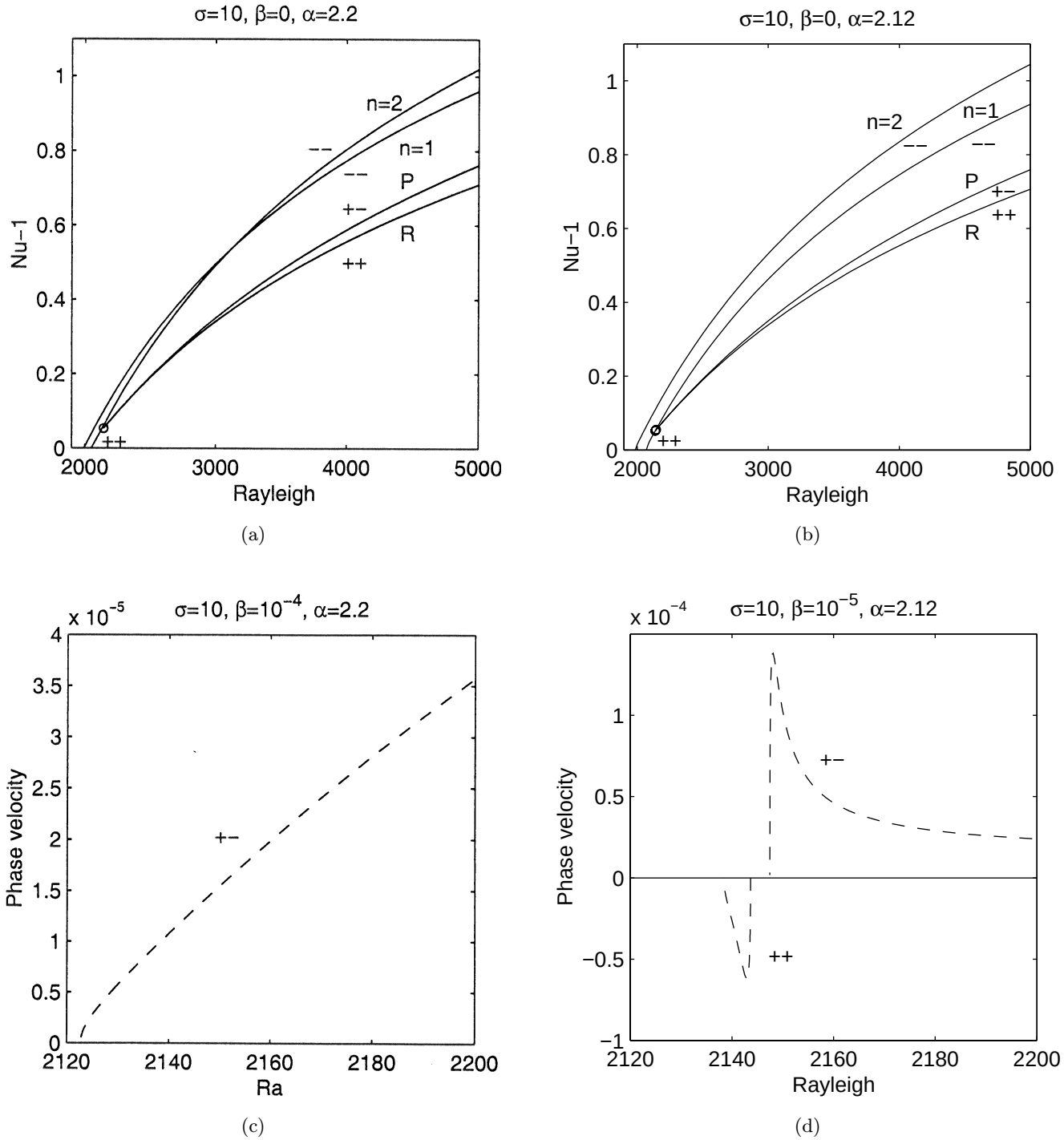

Fig. 3. Numerical results for $\sigma = 10$. (a) The Nusselt number $Nu - 1$ as a function of Ra for $\alpha = 2.2$, $\beta = 0$, (b) the same but for $\alpha = 2.12$, $\beta = 0$. (c) The phase velocity c of traveling waves as a function of Ra for $\alpha = 2.2$, $\beta = 10^{-4}$, (d) the same but for $\alpha = 2.12$, $\beta = 10^{-5}$. The sign of c is arbitrary since waves can always travel to the left or the right.

waves were found, even for values of α as close to α_c as $\alpha = 2.17$, in contrast to the case $\alpha < \alpha_c$ discussed below and the prediction of Armbruster [1987] for stress-free boundaries and $\sigma > 0.7$.

Figure 2(b) shows what happens when $\beta = 10^{-4}$. Although the $n = 1$ branch is essentially unaffected, the perturbation splits the multiple bifurcation from the $n = 2$ branch into two successive bifurcations. Both of these are to reflection symmetric states, hereafter referred to as R_1 and R_2 (see Sec. 4). The state corresponding to the P state now bifurcates in a tertiary steady state

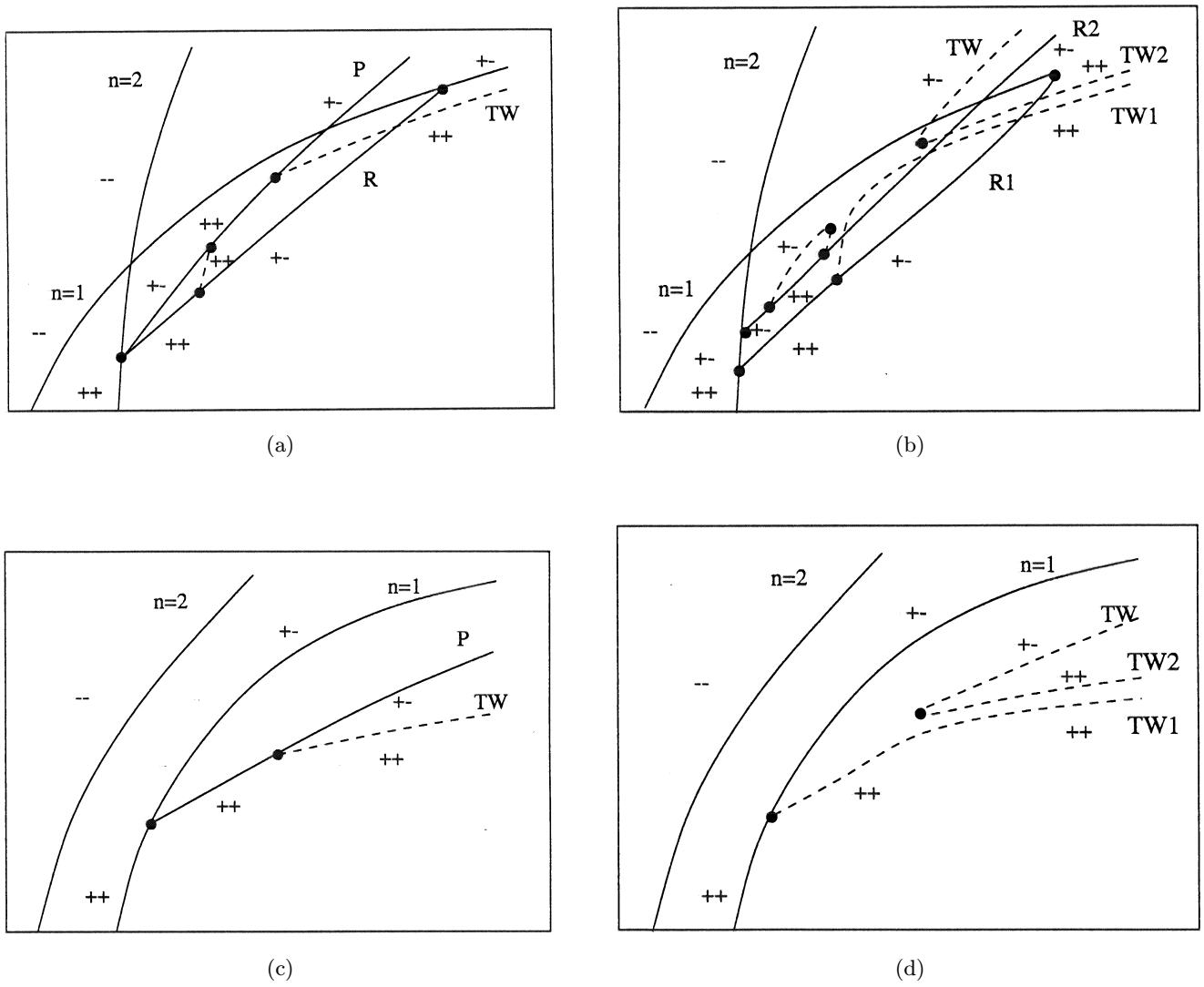

Fig. 4. Schematic bifurcation diagrams for $\sigma = 0.1$. (a) $\alpha = 2.2$, $\beta = 0$. (b) $\alpha = 2.2$, $\beta = 10^{-4}$. (c) $\alpha = 2.12$, $\beta = 0$. (d) $\alpha = 2.12$, $\beta = 10^{-4}$.

bifurcation from R_2 and is a *traveling wave*. Figure 3(c) shows that this bifurcation is a *parity-breaking* bifurcation, i.e. a steady state bifurcation from a circle of steady states that breaks the symmetry R. As a consequence the phase velocity of the TW vanishes at the tertiary bifurcation and increases away from it as the square root of the distance from the bifurcation (see, e.g. [Knobloch & Moore, 1990]). However, these solutions remain unstable.

Figures 2(c) and 2(d) show the corresponding results for $\alpha = 2.12 < \alpha_c$. When $\beta = 0$ the $n = 2$ mode now bifurcates first and again remains stable for all values of Ra. However, there are now two successive bifurcations from the initially unstable $n = 1$ branch whose combined effect is to stabilize the $n = 1$ branch at larger amplitudes [see Figs. 2(c) and 3(b)]. Moreover, in this case the predicted tertiary branch of traveling waves connecting the resulting R and P branches [Armbruster, 1987] is present, with the TW branch bifurcating from the P branch at $Ra = 2145.7$ and connecting to the R branch at $Ra = 2145.9$. We remark that for slightly smaller values of α the bifurcations to the R and P branches trade places and that in this process the TW branch disappears. An example for $\alpha = 2.08$ can be found in [Prat *et al.*, 1998], Fig. 8(a). Thus the predicted TW are present only very close to the mode interaction point. These important details are absent from Fig. 2 of [Armbruster, 1987].

Due to the presence of the TW the capture of the qualitative effects of symmetry breaking

requires that we use an even smaller value of β, viz. $\beta = 10^{-5}$. Figure 2(d) summarizes the results. These differ substantially from both Figs. 2(b) and 2(c), largely because of the behavior of the $n = 1$ branch. Behavior of this type is made possible because the $n = 1$ branch is a *mixed* mode when $\beta \neq 0$. As a result it can turn into other mixed mode branches with the same symmetry *without* a

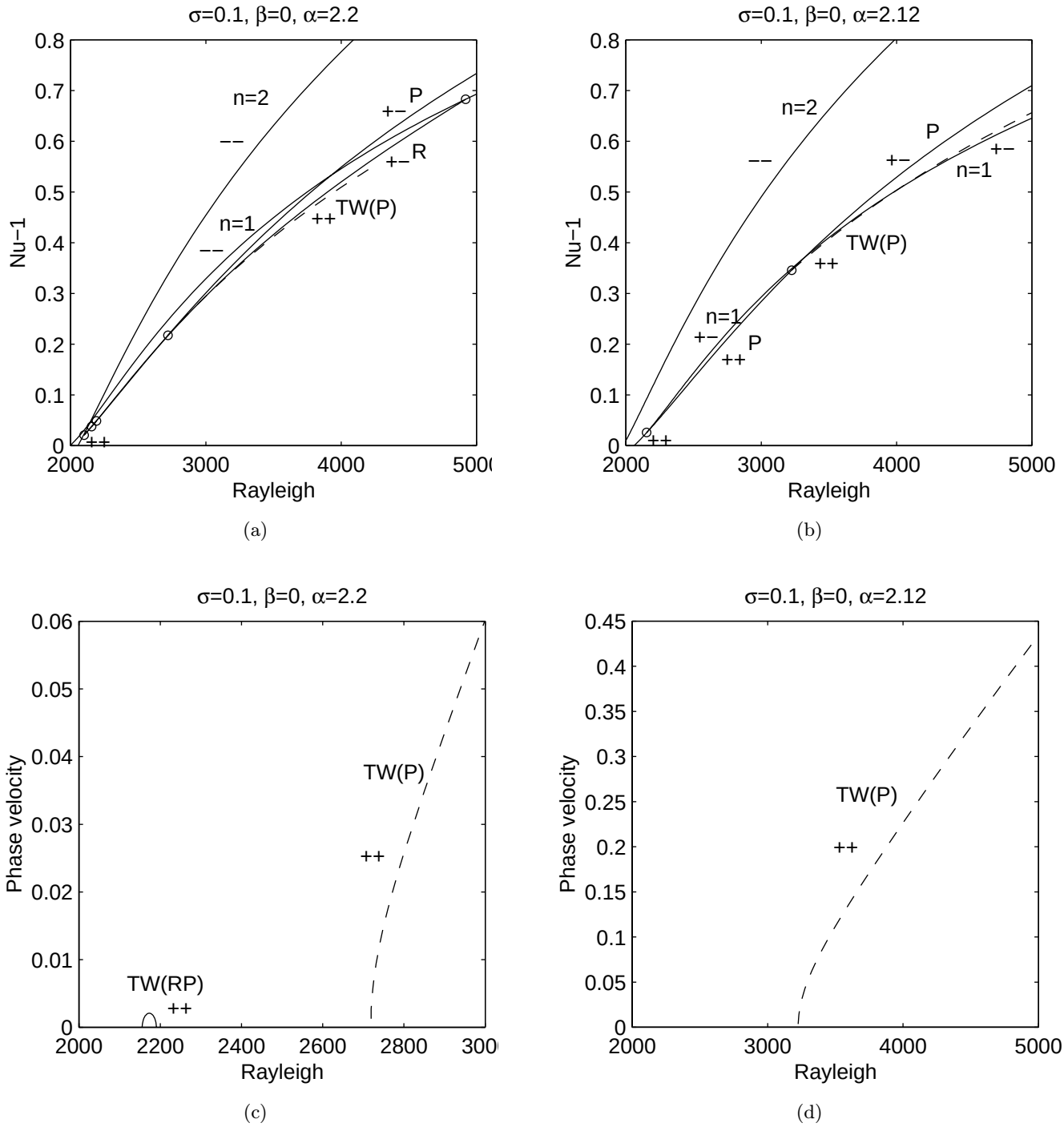

Fig. 5. Numerical results for $\sigma = 0.1$. (a and c) The Nusselt number $Nu - 1$ and the phase velocity c as functions of Ra for $\alpha = 2.2$, $\beta = 0$, (b and d) the same but for $\alpha = 2.12$, $\beta = 0$. (e and f) The phase velocity c as a function of Ra for $\alpha = 2.2$, $\beta = 10^{-4}$, (g) the same as (e) but for $\alpha = 2.12$, $\beta = 10^{-4}$. In (e) and (f) the notation $\mathrm{TW}(\mathrm{R}_1)$ refers to the branch TW_1 in Fig. 4(b). The sign of c is arbitrary since waves can always travel to the left or the right.

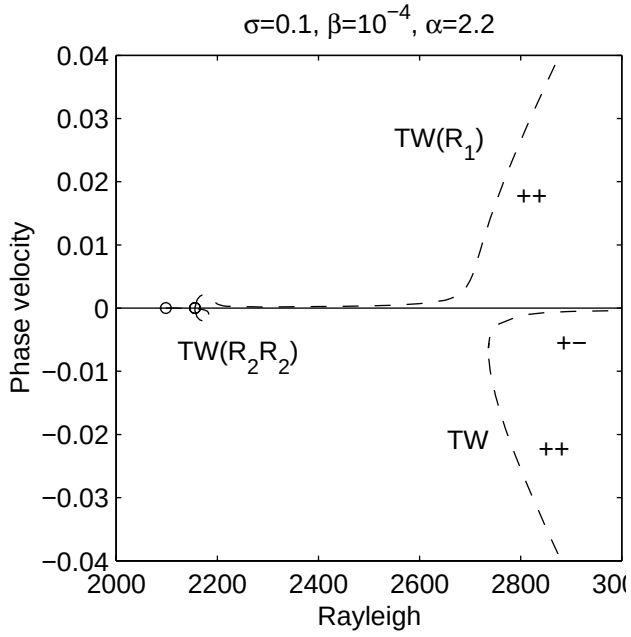

(e)

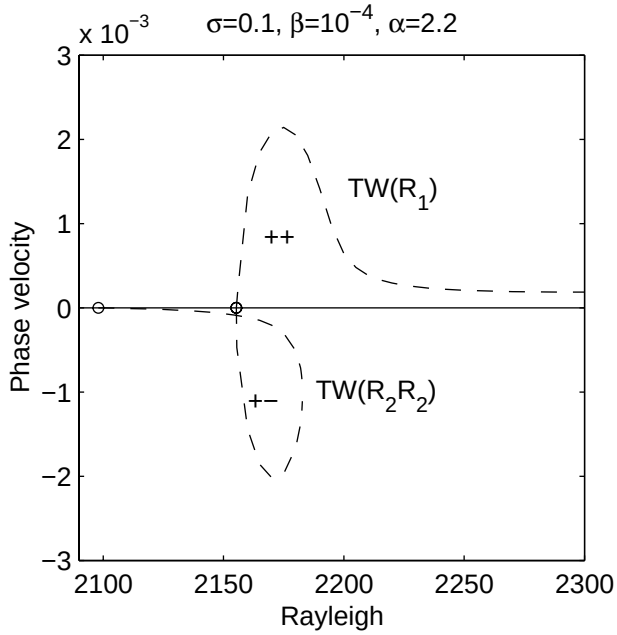

(f)

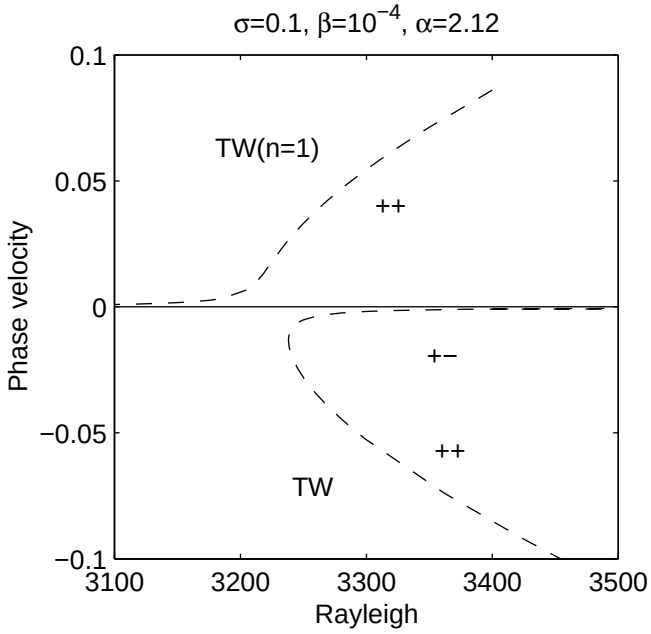

(g)

Fig. 5. (*Continued*)

bifurcation. As in Fig. 2(b) the branch R splits into two steady mixed mode branches R_1, R_2 while the P branch turns into a TW. The lower of the two $n = 1$ branches consists of an amalgam of the original $n = 1$ branch and R_1, and increases monotonically in amplitude. It possesses two secondary bifurcations connected by a secondary TW branch. The resulting bifurcation "bubble" [see Figs. 2(d) and 3(d)] is a consequence of the bifurcation to TW present on the R branch when $\beta = 0$, and consists in part of one of the resulting TW and in part the drifting P states. In contrast the upper $n = 1$ branch is

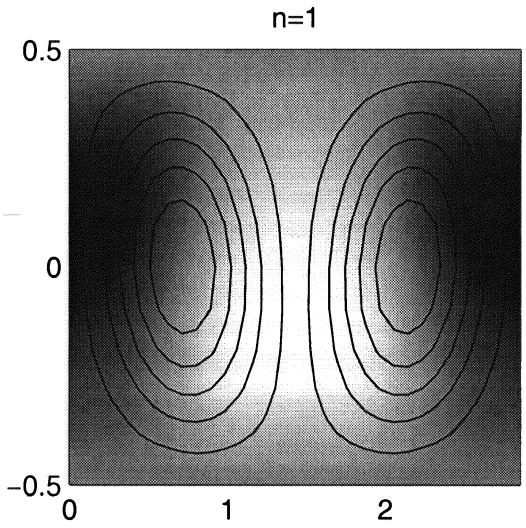

(a)

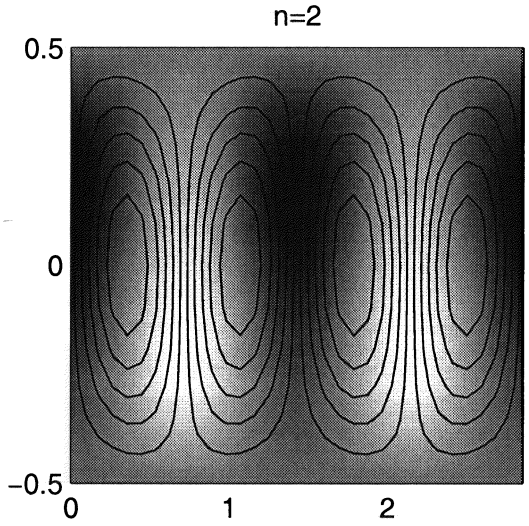

(b)

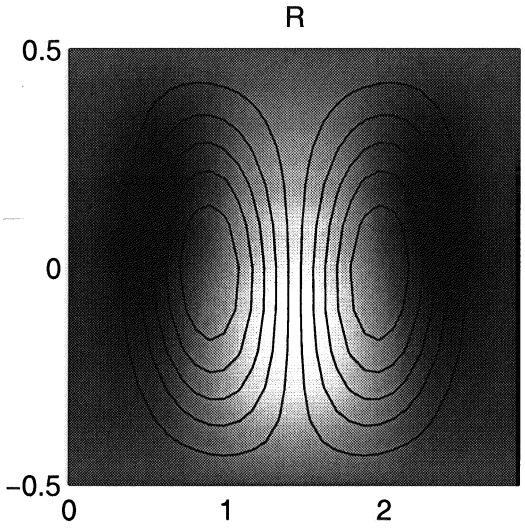

(c)

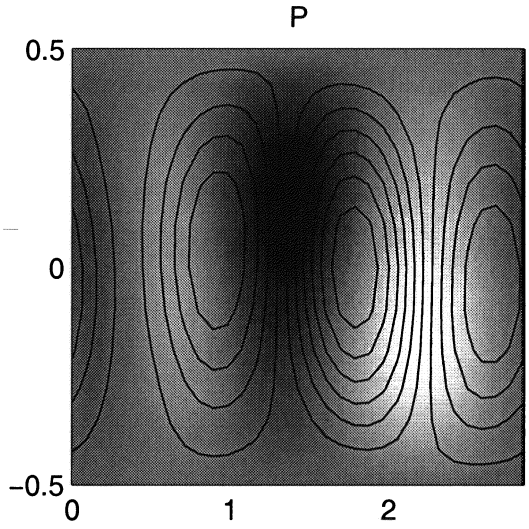

(d)

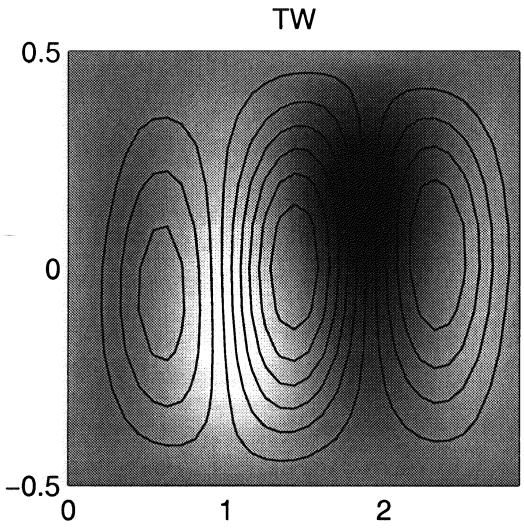

(e)

Fig. 6. Instantaneous streamlines of steady and traveling wave convection when $\beta = 0$, $\sigma = 0.1$, $\alpha = 2.2$ and $Ra = 3000$. Light (dark) shading indicates hot (cold) fluid. (a) The solution $n = 1$, (b) the solution $n = 2$, (c) the solution R, (d) the solution P, (e) the solution TW.

an amalgam of the upper part of the original $n = 1$ branch and the R_2 branch, connected via a saddle-node bifurcation. The large amplitude TW branch produced from the P branch bifurcates below the saddle-node [see Fig. 2(d)]. Consequently the whole of the $n = 1$ branch above the saddle-node is stable. As shown in Fig. 3(d) the phase velocity of the TW along this branch passes through a sharp maximum. This is a consequence of the fact that the initial part of this branch was a TW branch even when $\beta = 0$. Consequently the drift speed along this part of the branch is necessarily substantially larger than the slow drift of the P states that form the remainder of the TW branch caused by the weak breaking of the midplane reflection symmetry. Note that even with β small the computed bifurcation diagram lacks the expected the saddle-node bifurcation on one of the TW segments that should be inherited from the break-up of the TW present when $\beta = 0$. This is because the $\beta = 0$ TW branch is almost vertical [see Fig. 2(c)].

3.2. *Results for* $\sigma = 0.1$

For low Prandtl numbers the situation is more complex. Figure 4(a) summarizes the results for $\sigma = 0.1$, $\beta = 0$ and $\alpha = 2.2 > \alpha_c$. The basic features of this plot remain the same as for $\sigma = 10$, with two important differences. First, the R branch terminates on the $n = 1$ branch at $Ra = 4980$ with the $n = 1$ branch unstable at higher Rayleigh numbers. Two branches of TW are also present. A short segment in $2155 < Ra < 2190$, called TW(RP) in Fig. 5(c), connects the R and P branches, with a second bifurcation to TW occurring on the P branch at $Ra = 2710$. The latter produces the branch labeled TW(P) in Fig. 5(c). These bifurcations are all parity-breaking bifurcations from circles of reflection-symmetric states (i.e. from states with a symmetry that involves R) and so generate unstable TW via steady state bifurcation. These results differ from the predictions of Armbruster [1987] for $\sigma < 0.297$ and stress-free boundaries both in the presence of the TW branches and in the absence of a termination of the P branch.

As soon as the midplane reflection is broken the P branch becomes a TW while the multiple bifurcation on the $n = 2$ branch splits into two successive bifurcations to R-symmetric states, at $Ra = 2097.15$ and $Ra = 2097.20$, as for $\sigma = 10$ (see Sec. 4). However, the presence of the TW when $\beta = 0$ complicates this process considerably. Figure 4(b) shows what happens when $\beta = 10^{-4}$. What had been the P branch is now a TW branch that connects smoothly with the TW branches produced by the splitting of the original TW branches by the broken midplane reflection symmetry. As a result there is TW "bubble" on the R_2 branch in the range $2098 < Ra < 2155$ [called TW(R_2R_2) in Fig. 5(f)] with a saddle-node bifurcation at $Ra = 2183$. There is also a bifurcation to TW on the R_1 branch at $Ra = 2155$ with the resulting TW, called TW(R_1) in Fig. 5(f), extending to large Ra, and a disconnected segment, called TW in Fig. 5(e), with a saddle-node bifurcation at $Ra = 2736$. Figure 4(b) shows that the bifurcations to TW(R_1) and TW(R_2R_2) are distinct, despite the appearance of Fig. 5(f). The phase velocity plots are again simple to interpret; we emphasize that the sign of c is arbitrary and was chosen to be positive or negative for clarity only. For example, the TW branch that bifurcates from R_1 has initially a substantial phase velocity c because this part of the branch arises from the short TW segment in the $\beta = 0$ case [see Fig. 5(f)]. The phase velocity then drops to a small value because the middle part of the branch consists of drifting P states, before the phase velocity picks up again when the branch turns into TW_1, i.e. one of the TWs in the $\beta = 0$ case split by the small value of β [see Figs. 5(e) and 4(b)]. A similar argument applies to the disconnected TW branch in Fig. 4(b). In fact, our calculations indicate that at large Ra the phase velocity on what was the P branch may change sign, indicating that the corresponding TW drifts slowly in a direction opposite to that of the original TW. This is the case, for example, when $\beta = 0.01$. Of particular significance in what follows is the fact that the R_1 branch connects smoothly to the $n = 1$ branch. As a result the $n = 1$ branch has only a finite extent, $2010 < Ra < 4930$, before annihilation in a collision with the R_1 branch at $Ra = 4930$, and its role at large Ra is assumed by the R_2 branch.

Figures 4(c) and 4(d) show what happens when $\alpha = 2.12 < \alpha_c$. When $\beta = 0$ the $n = 2$ branch is stable throughout. The $n = 1$ branch is also supercritical but is unstable throughout, with a secondary bifurcation to an unstable P branch at $Ra = 2150$, followed by a tertiary bifurcation to unstable TW at $Ra = 3220$ [see Figs. 5(b) and 5(d)]. Once again this is a parity-breaking bifurcation from a circle of P states. The absence of an R branch is particularly noteworthy, since the $n = 1$ branch now remains unstable, eliminating the possibility of bistability

between the $n = 1$ and $n = 2$ branches. When $\beta = 10^{-4}$ the diagram breaks up in an obvious way [see Fig. 4(d)]: the P branch becomes a TW and the original TW splits into two, labeled TW_1 and TW_2, forming a branch of traveling waves that extends from a bifurcation on the $n = 1$ branch to large amplitudes, and a disconnected traveling wave branch formed from what was the large amplitude P branch and TW_2. As a result the former branch is composed of an initial part that is a drifting P state and hence is characterized by a relatively small value of c, followed at larger values of Ra for TW_1, i.e. a part that was a TW even in the unperturbed system, and hence is characterized by a substantially larger phase velocity [see Fig. 5(g)]. For the same reason we expect the phase velocity along the latter branch to drop dramatically near the saddle-node bifurcation as one traverses the disconnected branch towards larger amplitudes. Once again these results differ substantially from those of Armbruster for stress-free boundaries.

4. Interpretation of the Results

The results of the preceding section reveal three principal effects of breaking of the midplane reflection symmetry. First, the R branch splits into two branches, called R_1 and R_2. Second, the P branch begins to drift, forming a traveling wave with a small phase velocity, proportional to β. Third, the TW branch splits into two traveling wave branches, labeled TW_1 and TW_2. Using these observations it is a simple matter to construct the "unfolded" bifurcation diagrams.

In this section we explain the reason why the loss of midplane reflection leads to these effects. This is easiest done by identifying the corresponding transitions in the amplitude equations for the 1:2 mode interaction, although the conclusions obtained are valid quite generally. We suppose therefore that $(Ra - Ra_c)/Ra_c \ll 1$, $(\alpha - \alpha_c)/\alpha_c \ll 1$, and write the (total) streamfunction χ in the form

$$\chi(x,\, z,\, t) = \mathrm{Re}(ive^{ikx} + iwe^{2ikx})f(z) + \cdots .$$

Here $f(z)$ is the vertical eigenfunction, and v and w denote the complex amplitudes of the two modes. Since the system has $O(2)$ symmetry these amplitudes must satisfy equations equivariant with respect to the following two operations,

$$(v,\, w) \to (ve^{-ik\ell},\, we^{-2ik\ell})\,, \quad (v,\, w) \to (\overline{v},\, \overline{w})\,,$$

corresponding, respectively, to translations $x \to x + \ell$ of the origin and reflections $x \to -x$. The latter is a consequence of the fact that χ is a pseudoscalar under reflections. The most general equations satisfying this requirement take the form

$$\dot{v} = pv + qw\overline{v}\,, \quad \dot{w} = rw + sv^2\,,$$

where $p, \ldots, s$ are *real* invariant functions, i.e. functions of the three elementary invariants $|v|^2$, $|w|^2$ and $\mathrm{Re}\,\overline{v}^2 w$. To third order in the amplitudes we therefore have [Dangelmayr, 1986]

$$\dot{v} = \mu_1 v + a_1|v|^2 v + b_1|w|^2 v + c_1 w\overline{v}\,, \tag{3a}$$

$$\dot{w} = \mu_2 w + a_2|v|^2 w + b_2|w|^2 w + c_2 v^2\,. \tag{3b}$$

Here μ_1, μ_2 are the unfolding parameters. These equations are analyzed by Armbruster *et al.* [1988], and by Proctor and Jones [1988]. The equations possess pure $n = 2$ solutions of the form $(0,\, w)$ but no solutions of the form $(v,\, w) = (v,\, 0)$, i.e. no pure modes with $n = 1$. As a result the bifurcation at $\mu_1 = 0$ leads to a branch of *mixed* modes. Owing to translation invariance there is a whole circle of both solution types, with an associated zero eigenvalue. The pure $n = 2$ modes may lose stability to mixed modes of the form $(v,\, w)$, $vw \neq 0$, at which an additional simple eigenvalue passes through zero. Setting $v = r_1 e^{i\theta_1}$, $w = r_2 e^{i\theta_2}$ and $\psi = 2\theta_1 - \theta_2$, Eqs. (3) become

$$\dot{r}_1 = \mu_1 r_1 + a_1 r_1^3 + b_1 r_2^2 r_1 + c_1 r_1 r_2 \cos\,\psi\,, \tag{4a}$$

$$\dot{r}_2 = \mu_2 r_2 + a_2 r_1^2 r_2 + b_2 r_2^3 + c_2 r_1^2 \cos\,\psi\,, \tag{4b}$$

$$\dot{\theta}_1 = -c_1 r_2 \sin\,\psi\,, \quad \dot{\theta}_2 = \frac{c_2 r_1^2}{r_2}\sin\,\psi\,.$$

Thus

$$\dot{\psi} = -\left(\frac{c_2 r_1^2}{r_2} + 2c_1 r_2\right)\sin\,\psi\,. \tag{4c}$$

If we take $\theta_2 = 0$ the mixed modes take the form $\mathrm{M}_0 = (r_{1+},\, r_{2+})$, invariant under R_0, and $\mathrm{M}_\pi = (r_{1-}e^{i\pi/2},\, r_{2-})$, invariant under $R_{\pi/2k}$. These are the solutions R_1 and R_2 identified in Sec. 3. If $c_1 c_2 < 0$ these mixed modes can lose stability at a parity-breaking bifurcation to a TW. Such TW are fixed points of the relative phase ψ, although the individual phases $\dot{\theta}_1$, $\dot{\theta}_2$ drift in time. In particular, if $\mathrm{TW}^+ = \{r_1,\, r_2,\, \psi\}$ is a steady solution of Eqs. (4), so is $\mathrm{TW}^- = \{r_1,\, r_2,\, -\psi\}$. Since $\mathrm{TW}^- = R_0\mathrm{TW}^+$ the $\mathrm{TW}^\pm$ represent waves traveling in opposite directions, i.e. the parity-breaking bifurcation creates

waves that travel either to the left or to the right, depending on initial conditions. Hopf bifurcations from the mixed modes to standing waves can also occur but are not considered further since they do not occur in the PDEs.

The absence of a solution of the form $(v, w) = (v, 0)$, i.e. a pure $n = 1$ mode, is an important property of Eqs. (3). However, in the presence of midplane reflection symmetry the symmetry group of the problem is not $O(2)$ but $O(2) \times Z_2$. The midplane reflection $\kappa \in Z_2$ takes (v, w) into $(-v, -w)$ whenever $f(z)$ is even; otherwise it has no effect. Once again this is because the streamfunction χ is a pseudoscalar under reflections. Since $f(z)$ is even for the modes of interest here the extra reflection cannot be omitted. This requires a change in the amplitude equations describing the 1:2 resonance which now read [Armbruster, 1987]

$$\dot{v} = \mu_1 v + a_1|v|^2 v + b_1|w|^2 v + c_1 w^2 \overline{v}^3 \,, \quad (5a)$$

$$\dot{w} = \mu_2 w + a_2|v|^2 w + b_2|w|^2 w + c_2 v^4 \overline{w} \,. \quad (5b)$$

In these equations we have retained only the lowest order resonant terms; three other nonresonant fifth order terms in each equation have been omitted. Observe that the midplane reflection symmetry has had a dramatic effect on the structure of these equations. Pure $n = 1$ solutions $(v, 0)$ now exist. Moreover, mixed modes of the form (v, w), $vw \neq 0$, and symmetries R ($\psi = 0$) and P ($\psi = \pi/2$) bifurcate from both pure modes. The bifurcations from the $n = 1$ pure mode are due to simple zero eigenvalues, while that from the $n = 2$ pure mode is due to a double zero eigenvalue. Consequently, the mixed modes bifurcate in succession from the $n = 1$ pure mode but simultaneously from the $n = 2$ modes, in agreement with the numerical results of Sec. 3.

Equations (5) can be written in the alternative form

$$\dot{r}_1 = \mu_1 r_1 + a_1 r_1^3 + b_1 r_2^2 r_1 + c_1 r_1^3 r_2^2 \cos 2\psi \,, \quad (6a)$$

$$\dot{r}_2 = \mu_2 r_2 + a_2 r_1^2 r_2 + b_2 r_2^3 + c_2 r_1^4 r_2 \cos 2\psi \,, \quad (6b)$$

$$\dot{\psi} = -r_1^2(c_2 r_1^2 + 2c_1 r_2^2) \sin 2\psi \,, \quad (6c)$$

showing the presence of mixed modes with $\psi = 0$, $\pi/2$, π, $3\pi/2$. If $\theta_2 = 0$, the mixed mode $\mathrm{M}_0 = (r_{1+}, r_{2+})$ is invariant under R_0, $\mathrm{M}_{\pi/2} = (r_{1-}e^{i\pi/4}, r_{2-})$ is invariant under $P = R_{3\pi/4k} T_{\pi/k} \kappa$, while M_π, $\mathrm{M}_{3\pi/2}$ are related to M_0 and $\mathrm{M}_{\pi/2}$ using appropriate symmetries: $\mathrm{M}_\pi = (r_{1+}e^{i\pi/2}, r_{2+}) = \kappa R_0 T_{-\pi/2k} \mathrm{M}_0$, $\mathrm{M}_{3\pi/2} = (r_{1-}e^{i3\pi/4}, r_{2-}) = T_{-\pi/k} R_0 \mathrm{M}_{\pi/2}$. Here R_{l_0} is defined to be $T_{l_0} R_0 T_{-l_0}$, as before.

The effects of weak breaking of the midplane reflection symmetry can be incorporated by including in Eqs. (5) small quadratic terms:

$$\dot{v} = \mu_1 v + a_1|v|^2 v + b_1|w|^2 v + \beta_1 w\overline{v} + c_1 w^2 \overline{v}^3 \,,$$

$$\dot{w} = \mu_2 w + a_2|v|^2 w + b_2|w|^2 w + \beta_2 v^2 + c_2 v^4 \overline{w} \,,$$

where β_1, β_2 are both of order β. Although the detailed properties of these equations will be reported elsewhere, we use them here to identify the origin of the splitting of the R and TW branches observed in Figs. 2 and 4 when $0 < \beta \ll 1$, as well as the origin of the drift of the P states.

In the (r_1, r_2, ψ) variables these equations become

$$\dot{r}_1 = \mu_1 r_1 + a_1 r_1^3 + b_1 r_2^2 r_1 + \beta_1 r_1 r_2 \cos\psi + c_1 r_1^3 r_2^2 \cos 2\psi \,, \quad (7a)$$

$$\dot{r}_2 = \mu_2 r_2 + a_2 r_1^2 r_2 + b_2 r_2^3 + \beta_2 r_1^2 \cos\psi + c_2 r_1^4 r_2 \cos 2\psi \,, \quad (7b)$$

$$\dot{\psi} = -\left(\frac{\beta_2 r_1^2}{r_2} + 2\beta_1 r_2\right) \sin\psi - r_1^2(c_2 r_1^2 + 2c_1 r_2^2) \sin 2\psi \,. \quad (7c)$$

Consequently, when β is small but nonzero the steady mixed modes are those corresponding to M_0, M_π and these are now split, i.e. they are no longer related by the symmetry $\kappa R_0 T_{-\pi/2k}$. In contrast the modes corresponding to $\psi = \pi/2$, $3\pi/2$ are perturbed to a single TW. This is because for each fixed point of Eqs. (7) of the form $\{r_1, r_2, \psi = \pi/2 + \varepsilon\}$ there is also a fixed point $\{r_1, r_2, \psi = 3\pi/2 - \varepsilon\}$ (with the same r_1, r_2) and these solutions are related by the remaining symmetries: $\mathrm{TW}_{\pi/2+\varepsilon} = (r_1 e^{i(\pi/4+\varepsilon/2+\theta_2/2)}, r_2 e^{i\theta_2})$, and $\mathrm{TW}_{3\pi/2-\varepsilon} = (r_1 e^{i(3\pi/4-\varepsilon/2-\theta_2/2)}, r_2 e^{-i\theta_2}) = T_{-\pi/k} R_0 \mathrm{TW}_{\pi/2+\varepsilon}$. Here $c = \dot{\theta}_2/2k = \dot{\theta}_1/k$ is the phase velocity of the wave and is small.

Likewise, observe that Eqs. (6) admit TW solutions provided $c_1 c_2 < 0$ and $\sin 2\psi \neq 0$. It follows that if $\{r_1, r_2, \psi = \delta\}$ solves (6) so does $\{r_1, r_2, \psi = \pi - \delta\}$. Consequently, there are two types of traveling wave solutions of the system (5), $\mathrm{TW}_1 = (r_1 e^{i(\delta+\theta_2)/2}, r_2 e^{i\theta_2})$ and $\mathrm{TW}_2 = (r_1 e^{i(\pi-\delta-\theta_2)/2}, r_2 e^{-i\theta_2})$, related by the symmetry $\kappa T_{\pi/2k} R_0 \in D_2$: $\kappa T_{\pi/2k} R_0 \mathrm{TW}_1 = \mathrm{TW}_2$. It follows therefore that when the midplane symmetry κ is

broken these two solutions become distinct, i.e. the TW branch splits into two once β becomes nonzero. Note that $\mathrm{TW}_3 = (r_1 e^{-i(\delta+\theta_2)/2},\ r_2 e^{-i\theta_2})$ is another TW with the property that $R_0\mathrm{TW}_3 = \mathrm{TW}_1$, i.e. TW_1 and TW_3 form a pair of left- and right-traveling waves of type TW_1, and similarly for TW_2 and $\mathrm{TW}_4 = (r_1 e^{i(3\pi+\delta+\theta_2)/2},\ r_2 e^{i\theta_2})$.

5. Discussion

In this paper we have discussed and illustrated the consequences of weak breaking of the midplane reflection symmetry on the 1:2 mode interaction in Rayleigh–Bénard convection. We identified three basic principles that enabled us to determine the consequences of such symmetry breaking. These consisted of the splitting of the branches of R and TW solutions, and of the appearance of a slow drift in the P solutions. As a result the P solutions become traveling waves and can connect with the traveling waves produced by the splitting of the original TW branches. Likewise, the splitting of the mixed modes R allows the hybrid $n = 1$ solution branch to connect with them. Although these results were based on the form of the solutions of the corresponding amplitude equations they are in fact only based on the symmetry properties of these solutions. Consequently they apply in a wider parameter regime than required for the validity of the mode interaction equations. In fact the derivation of these equations is valid only in the neighborhood of the codimension two point $(Ra_c,\ \alpha_c)$ and for sufficiently weak breaking of the midplane reflection symmetry. In this derivation the two unfolding parameters μ_1, μ_2 enter in the linear terms only, while the symmetry breaking parameter β enters only in the coefficients of the small quadratic terms. Under appropriate nondegeneracy conditions the cubic and quintic term coefficients can be calculated *at* the multiple bifurcation point (i.e. at $\mu_1 = \mu_2 = 0$) and at $\beta = 0$ and hence are *independent* of both the Rayleigh number and the spatial period. However, as in other applications, it is not possible to state *a priori* the size of the neighborhood of the mode interaction point in which the resulting equations remain valid. Thus it should be of no surprise that for any given set of parameters the results for the partial differential equations may differ from the normal form predictions. Wittenberg and Holmes [1997] discussed in detail an example of this type. For this reason the full partial differential equations must be used to identify the correct dynamics away from the codimension two point and to trace the transition from weak to strong resonance as the strength of the midplane symmetry breaking terms is progressively increased. Note, however, that Eqs. (7) suggest that the transition between the two extreme cases occurs already at $\beta \sim \varepsilon^{3/2}$, where ε indicates the distance in the $(Ra,\ \alpha)$ plane from $(Ra_c,\ \alpha_c)$, i.e. for $\beta \ll 1$. Although these results could have been anticipated without solving the full partial differential equations the calculations provide valuable additional information, because they allow us to estimate the size of the interval in β in which such a theory applies, while at the same time providing a visualization of the various possible solutions. The above estimate suggests that for the values of α used the transition between behavior characteristic of weak and strong 1:2 resonance should occur for $\beta \approx 0.01$. In fact we have seen that in the case of $\sigma = 10$ values of β as small as 10^{-5} were not small enough to yield the generic unfolding of the weak resonance. We found that this limitation was due to the presence of certain secondary branches (in this case TW) that turned out to be almost degenerate. Indeed, this investigation was motivated in part by our inability to understand the bifurcation diagrams for $\beta = 10^{-2}$ which we had assumed to be "small" on the basis of the heuristic argument just given. In contrast, Manogg and Metzener [1994] considered, at the level of the amplitude equations, the regime $\beta \sim \varepsilon^{1/2}$. As a result of this larger symmetry breaking their bifurcation diagrams do not collapse into those of Ambruster [1987] as $\beta \to 0$, leaving the origin of much of the reported behavior mysterious. It should be pointed out that not all mode interactions are affected equally by the loss of midplane reflection symmetry. For example, weak symmetry breaking has almost no effect on the 1:3 interaction; this interaction is therefore still expected to dominate the process of wavenumber selection at moderate Rayleigh numbers, as it does in the presence of midplane reflection symmetry [Prat *et al.*, 1998].

The principles identified above will be used in a future publication to elucidate the effects on the 1:2 resonance of heat loss from the top boundary via Newton's law of cooling, and to identify parameter regimes in which nontrivial dynamics may result. More generally, calculations of this type serve to quantify the imperfection tolerance of idealized

models of physical systems and hence the reliability of any predictions that are based on them.

Acknowledgments

We are grateful to Joan Sánchez for assistance with numerical continuation. This work was supported in part by DGESIC under grant PB97-0683 (I. Mercader and J. Prat) and by the National Science Foundation under grant DMS-9703684 (E. Knobloch). We thank the Fulbright Foundation for additional support.

References

Armbruster, D. [1987] "O(2)-symmetric bifurcation theory for convection rolls," *Physica* **D27**, 433–439.

Armbruster, D., Guckenheimer, J. & Holmes, P. [1988] "Heteroclinic cycles and modulated traveling waves in systems with O(2) symmetry," *Physica* **D29**, 257–282.

Busse, F. H. [1967] "The stability of finite amplitude cellular convection and its relation to an extremum principle," *J. Fluid Mech.* **30**, 625–649.

Busse, F. H. & Or, A. C. [1986] "Subharmonic and asymmetric convection rolls," *Z. Angew. Math. Phys.* **37**, 608–623.

Clever, R. M. & Busse, F. H. [1996] "Hexagonal convection cells under conditions of vertical symmetry," *Phys. Rev.* **E53**, R2037–R2040.

Cox, S. M. [1996] "Mode interactions in Rayleigh–Bénard convection," *Physica* **D95**, 50–61.

Crawford, J. D. & Knobloch, E. [1991] "Symmetry and symmetry-breaking bifurcations in fluid mechanics," *Ann. Rev. Fluid Mech.* **23**, 341–387.

Dangelmayr, G. [1986] "Steady-state mode interaction in the presence of O(2)-symmetry," *Dyn. Stab. Syst.* **1**, 159–185.

Echebarría, B., Krmpotić, D. & Pérez-García, C. [1997] "Resonant interactions in Bénard–Marangoni convection in cylindrical containers," *Physica* **D99**, 487–502.

Golubitsky, M., Swift, J. W. & Knobloch, E. [1984] "Symmetries and pattern selection in Rayleigh–Bénard convection," *Physica* **D10**, 249–276.

Holmes, P., Lumley, J. L. & Berkooz, G. [1996] *Turbulence, Dynamical Systems and Symmetry* (Cambridge University Press, Cambridge).

Jones, C. A. & Proctor, M. R. E. [1987] "Strong spatial resonance and travelling waves in Bénard convection," *Phys. Lett.* **A121**, 224–228.

Knobloch, E. & Moore, D. R. [1990] "A minimal model of binary fluid convection," *Phys. Rev.* **A42**, 4693–4709.

Knobloch, E. [1996] "Symmetry and instability in rotating hydrodynamic and magnetohydrodynamic flows," *Phys. Fluids* **8**, 1446–1454.

Manogg, G. & Metzener, P. [1994] "Strong resonance in two-dimensional non-Boussinesq convection," *Phys. Fluids* **6**, 2944–2955.

Matthews, P. C., Hurlburt, N. E., Proctor, M. R. E. & Brownjohn, D. P. [1992] "Compressible magnetoconvection in oblique fields: Linearized theory and simple nonlinear models," *J. Fluid Mech.* **240**, 559–569.

Moore, D. R., Weiss, N. O. & Wilkins, J. M. [1991] "Asymmetric oscillations in thermosolutal convection," *J. Fluid Mech.* **233**, 561–585.

Prat, J., Massaguer, J. M. & Mercader, I. [1995] "Large-scale flows and resonances in 2-D thermal convection," *Phys. Fluids* **7**, 121–134.

Prat, J., Mercader, I. & Knobloch, E. [1998] "Resonant mode interactions in Rayleigh–Bénard convection," *Phys. Rev.* **E58**, 3145–3156.

Proctor, M. R. E. & Jones, C. A. [1988] "The interaction of two spatially resonant patterns in thermal convection, Part 1. Exact 2:1 resonance," *J. Fluid Mech.* **188**, 301–335.

Weiss, N. O. [1990] "Symmetry breaking in nonlinear convection," in *Nonlinear Evolution of Spatio-Temporal Structures in Dissipative Continuous Systems*, eds. Busse, F. H. & Kramer, L. (Plenum Press, NY), pp. 359–374.

Wittenberg, R. & Holmes, P. [1997] "The limited effectiveness of normal forms: A critical review and extension of local bifurcation studies of the Brusselator PDE," *Physica* **D100**, 1–40.